

Lithium Cepheid V708 Car with an unusual chemical composition

V. V. Kovtyukh^{1,2}, S. M. Andrievsky^{1,3}, K. Werner², S. A. Korotin⁴, and A. Y. Kniazev^{5,6}

¹ Astronomical Observatory, Odessa National University, Shevchenko Park, 65014, Odessa, Ukraine
e-mail: vkovtyukh@ukr.net

² Institut für Astronomie und Astrophysik, Kepler Center for Astro and Particle Physics, Universität Tübingen, Sand 1, 72076 Tübingen, Germany

³ GEPI, Observatoire de Paris, Université PSL, CNRS, 5 Place Jules Janssen, F-92190 Meudon, France

⁴ Physics of stars department, Crimean Astrophysical Observatory, Nauchny 298409, Republic of Crimea

⁵ South African Astronomical Observatory, PO Box 9, 7935 Observatory, Cape Town, South Africa

⁶ Southern African Large Telescope Foundation, PO Box 9, 7935 Observatory, Cape Town, South Africa

Received date; accepted: date

ABSTRACT

Aims. The purpose of this work is to spectroscopically analyse the classical Cepheid V708 Car. A preliminary check of the spectrum of V708 Car showed that this is a lithium-rich supergiant. We also found that V708 Car has an unusual chemical composition in that the abundances of various elements correlate with their condensation temperatures. We tried to find an explanation of this feature, which is unusual for classical Cepheids.

Methods. For the spectroscopic analysis, we used methods based on the assumption of local and non-local thermodynamic equilibrium.

Results. We determined the fundamental parameters of our program star V708 Car. This long-period Cepheid has a mass of about $12 M_{\odot}$. We derived the abundances of 27 chemical elements in this star. They are clearly correlated with their condensation temperature: the higher the condensation temperature, the lower the abundance (there are exceptions for sodium and barium, however). We explain this peculiar chemical composition of the V708 Car atmosphere by the gas–dust separation in the envelope of this star. A similar mechanism leads to the observed peculiarities of the chemical composition of λ Boo, W Vir, and asymptotic giant branch stars.

Key words. stars: abundances – stars: variables: Cepheids – stars: individual: V708 Car – stars: evolution

1. Introduction

Classical Cepheids are pulsating supergiant stars with spectral classes from F to K. They pulsate in radial mode(s). The pulsational instability of a Cepheid occurs when the star enters the so-called instability strip (IS) in the Hertzsprung–Russell (HR) diagram before and after a previous red giant stage. The progenitors of Cepheids in the main-sequence (MS) stage are O-B type stars, whose masses range from approximately 3 to $20 M_{\odot}$ or more.

V708 Car was classified as a classical Cepheid with a pulsation period $P = 51.4$ d (ASAS project; Pojmanski 2002). Later, Berdnikov (2010) confirmed this classification. V708 Car is a poorly investigated Cepheid. The SIMBAD database lists only eight publications related to the study of this star. These papers are mainly devoted to photometric studies. Berdnikov (2010) also performed a search for evolutionary changes in V708 Car using the Harvard photographic plate collection and CCD observations. He found that the pulsational period increases by about 52 s/yr.

V708 Car is a rather massive Cepheid. From its position in the HR diagram (see discussion below), its mass should be about $12 M_{\odot}$, while its bolometric absolute magnitude is -6.03 mag. Based on the period–luminosity relation by Breuval et al. (2022), the luminosity of the star is about $18\,400 L_{\odot}$ (using the correction for $[\text{Fe}/\text{H}] = -0.40$).

2. Observations and data reduction

Spectral observations of V708 Car were made on 2016 June 8 at a pulsation phase of 0.216 with the High Resolution Fibre échelle Spectrograph (HRS) (HRS; Barnes et al. 2008; Bramall et al. 2010, 2012; Crause et al. 2014) at the Southern African Large Telescope (SALT; Buckley et al. 2006; O’Donoghue et al. 2006). The HRS is a thermostabilised double-beam échelle spectrograph whose entire optical part is housed in vacuum to reduce temperature and mechanical influences. The blue arm of the spectrograph covers the spectral range of 3735–5580 Å, and the red arm covers the spectral range of 5415–8870 Å. The spectrograph can be used in low-resolution (LR, with a resolving power $R \approx 14\,000 - 15\,000$), medium-resolution (MR, $R \approx 36\,500 - 39\,000$), and high-resolution (HR, $R \approx 67\,000 - 74\,000$) modes and is equipped with two fibers (object and sky fibers) for each mode. During the observations of V708 Car, the MR mode was used with fibers of 2’’23 in diameter. The CCD detectors for the blue and red arms were used with a binning of 1×1 .

The primary HRS data reduction was performed automatically using the SALT standard pipeline (Crawford et al. 2010), and the subsequent échelle data reduction was made using the HRS pipeline, as described in detail in Kniazev et al. (2019).

3. Atmosphere parameters of V708 Car and its chemical composition

The effective temperature T_{eff} of V708 Car was derived from the line-depth ratios (Kovtyukh 2007). This technique is commonly used in studies of Cepheid variables (e.g. Andrievsky et al. 2016, Luck 2018, Lemasle et al. 2018, da Silva et al. 2022, Kovtyukh et al. 2022). When T_{eff} was determined, the surface gravity ($\log g$) was found by imposing the iron ionisation balance (the same iron abundance as derived from the neutral and ionised lines). The microturbulent velocity V_t was derived assuming that there is no dependence between the iron abundance obtained from the Fe I lines and their equivalent widths (EWs; Fig. 1). The adopted abundance value $[\text{Fe}/\text{H}]$ was derived from the Fe I lines because we assumed ionisation balance and because they outnumber the Fe II lines. The atmospheric parameters T_{eff} , $\log g$, and V_t are listed in Table 1, together with some other parameters of the program star.

3.1. Local thermodynamic equilibrium results

The abundances of different elements were derived in the local thermodynamic equilibrium (LTE) approximation using the atmosphere model computed with ATLAS9 code by Castelli & Kurucz (2003) for the atmosphere parameters. The oscillator strengths, $\log gf$, were adopted from the Vienna Atomic Line Database (VALD, Ryabchikova et al. 2015, version 2023). The reference solar abundances were taken from Asplund et al. (2009).

3.2. Non-local thermodynamic equilibrium results

For eight chemical elements, we applied the non-LTE (NLTE) approximation to derive their abundances. The atomic models that were used are described in detail in several papers, for example, carbon (Andrievsky et al. 2001, Lyubimkov et al. 2015), sodium (Korotin & Mishenina 1999, Dobrovolskas et al. 2014), magnesium (Mishenina et al. 2004, Černiauskas et al. 2017), aluminum (Andrievsky et al. 2008, Caffau et al. 2019), sulfur (Korotin 2009, and barium (Andrievsky et al. 2009).

The general method of the NLTE calculations is the following. In order to find atomic level populations for the ions of interest, we employed the code MULTI (Carlsson 1986). This program was modified by Korotin et al. (1999). MULTI allows us to calculate a single NLTE line profile. When the line of interest was blended, we performed the following procedure. With the help of MULTI, we first calculated the departure coefficients for the atomic levels that cause the formation of the considered line. After this, we included these coefficients in the LTE synthetic spectrum code SYNTHV (Tsymbal et al. 2019). This allowed us to calculate the source function and opacity for each studied line. Simultaneously, the blending lines were calculated in LTE with the help of the line list and corresponding atomic data from the VALD database (Ryabchikova et al. 2015) in the wavelength range of the line under study. For all our computations, we used 1D LTE atmosphere models computed with the ATLAS9 code by Castelli & Kurucz (2003). In Tables 2 and 3, we list the resulting LTE and NLTE elemental abundances in V708 Car.

The star is not so far away from the Sun. Its heliocentric distance is only about 4.4 kpc (Gaia EDR3, Gaia Collaboration et al. 2021). The same distance results from the period–luminosity relation (Wang et al. 2018, see Skowron et al. 2019 for details). The galactocentric distance is 8 kpc. Therefore, the decreased iron abundance in this star could

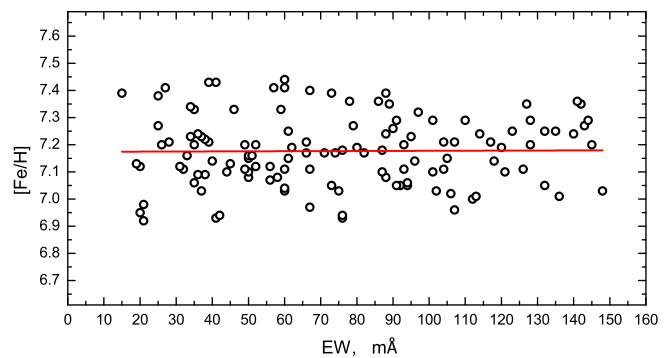


Fig. 1. V_t determination (absence of a dependence between the iron abundance of individual lines and their equivalent widths).

mean that it is a thick-disc Cepheid, but its distance below the Galactic plane is only -185 pc, which means that it could also be a member of the thin-disc population.

3.3. Lithium in V708 Car

Fig. 2 shows the Li I 6707.8 Å spectral line in our program Cepheid. High lithium abundances are very rare in supergiant stars because the lithium nuclei are destroyed by reactions with protons at the bottom of the convection zone. Nevertheless, some examples of lithium-rich supergiants exist. For instance, the F-type supergiant HD 172365 was discovered by Luck (1982) as a high Li abundance star. Andrievsky et al. (1999) found in a spectroscopic study that the lithium abundance in this star is $\log A(\text{Li}) = 2.9$. These authors discussed the properties of this supergiant and concluded that HD 172365 may be a post-blue straggler star with a mass about twice as high as the turn-off point mass for the open cluster IC 4756, of which HD 172365 is a member. This star could be formed by a merger process of two companions of a close binary system. Another supergiant, HD 174104, was also described as lithium rich by Luck (1982).

While non-variable supergiants are situated near or outside the instability strip, some pulsating yellow supergiant Cepheids also show an increased lithium abundance. The first lithium-rich Cepheid HV 5497 from the Large Magellanic Cloud was described by Luck & Lambert (1992). Luck & Lambert (2011) reported increased lithium level in the Cepheid V1033 Cyg, and Kovtyukh et al. (2016) indicated that the lithium abundance in the Cepheid V371 Per is high. Three Cepheids with a high lithium abundance were described by Kovtyukh et al. (2019) (namely, ASAS 075842-2536.1 and ASAS 131714-6605.0), and OGLE GD-CEP-0516 (Kovtyukh 2023). All have solar metallicity and $\log A(\text{Li})$ of about 3.0. Tables 4 and 5 list some characteristics of the lithium-rich Cepheids and non-variable stars.

Fig. 3 shows a HR diagram in which the position of our program Cepheid is indicated, as well as the positions of other lithium-rich Cepheids and non-variable supergiants discussed above. To determine the luminosity, the period–luminosity relation was used, and metallicity was taken into account (Breuval et al. 2022). It should be noted that all Cepheids (within the measurement error) are situated near the edges of the instability strip. We have to remark that Berdnikov (2010) argued that V708 Car is a Cepheid that is crossing the instability strip for the third time. If we accept this supposition, then it is very difficult to explain the high lithium abundance in this star because in this case, it should already have experienced the first and second dredge-up episodes. We leave this question open for now.

Table 1. Moment in time of the spectroscopic observation and model parameters of V708 Car.

JD	P, days	phase	T_{eff} , K	$\log g$	V_t , km s $^{-1}$	[Fe/H]
2457547.738	51.403084	0.216	5206	1.30	4.30	-0.40

Table 2. LTE elemental abundances in V708 Car.

Ion	[El/H]	σ	NL	(El/H)	T_{cond} , K
Li I	+0.79	0.20	1	1.95	1142
C I	-0.32	0.11	1	8.36	40
O I	+0.08	0.13	2	9.06	180
Na I	+0.21	0.20	1	6.53	958
Mg I	-0.28	0.20	1	7.40	1354
Al I	-0.29	0.31	3	6.01	1653
Si I	-0.31	0.08	14	7.29	1354
S I	+0.10	0.17	2	7.31	664
Ca I	-0.60	0.06	6	5.78	1517
Sc II	-0.87	0.11	5	2.38	1659
Ti I	-0.66	0.26	12	4.37	1582
Ti II	-0.93	0.13	2	4.11	1582
V I	-0.68	0.10	3	3.43	1429
V II	-0.55	0.02	2	3.57	1429
Cr I	-0.54	0.07	11	5.22	1296
Cr II	-0.25	0.08	4	5.51	1296
Mn I	-0.29	0.21	6	5.25	1158
Fe I	-0.40	0.12	141	7.18	1334
Fe II	-0.39	0.10	16	7.19	1334
Co I	-0.59	0.16	4	4.40	1352
Ni I	-0.45	0.17	30	5.85	1353
Cu I	-0.33	0.16	2	3.96	1037
Zn I	+0.34	0.21	1	4.79	726
Y II	-0.72	0.02	4	1.47	1659
Zr II	-1.05	0.22	1	1.83	1741
La II	-0.47	0.13	6	0.86	1578
Ce II	-0.56	0.22	6	1.15	1478
Pr II	-0.81	0.14	3	0.00	1582
Nd II	-0.57	0.20	7	0.95	1602
Sm II	-0.42	0.11	3	0.68	1590
Eu II	-0.18	0.22	1	0.78	1356

Remarks:

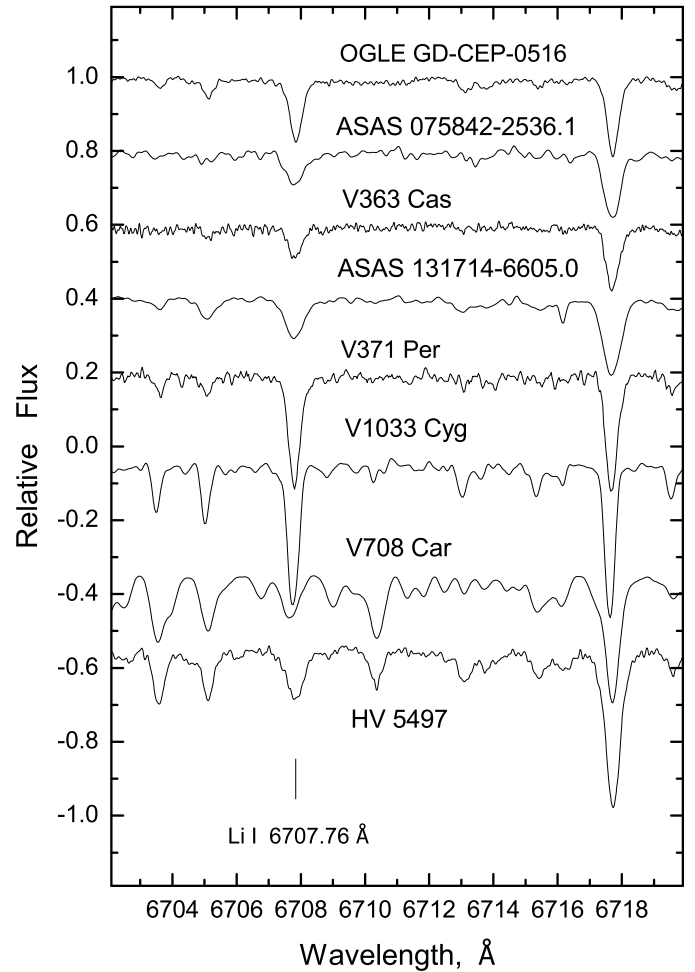
NL is the number of lines used,
 [El/H] is the abundance relative to the solar value,
 (El/H) is the absolute abundance value on a scale where the hydrogen abundance is 12.00,
 T_{cond} is the condensation temperature.

Table 3. NLTE elemental abundances in V708 Car.

Ion	(El/H)	σ	NL	[El/H]	Sun	T_{cond} , K
C I	8.10	0.12	5	-0.33	8.43	40
O I	8.88	0.10	4	+0.16	8.71	180
Na I	6.29	0.05	6	+0.04	6.25	958
Mg I	7.03	0.15	5	-0.51	7.54	1354
Al I	5.90	0.20	3	-0.53	6.43	1653
S I	7.10	0.12	4	-0.06	7.16	664
Cu I	4.05	0.10	4	-0.20	4.25	1037
Ba II	2.34	0.10	4	-0.17	2.17	1455

Remarks:

For the Sun, our NLTE abundances are listed.


Fig. 2. Lithium line in the spectrum of V708 Car and other lithium-rich Cepheids.

It is interesting to note that the lithium-rich Cepheids include five double-mode pulsators. Double-mode Cepheids form a rare group of classical Cepheids. They simultaneously pulsate in either in the second P_2 and first P_1 overtones or in the first overtone and fundamental mode P_0 (Table 4).

4. Chemical composition peculiarities of V708 Car and their possible origins

Fig. 4 shows the results of our abundance measurements relative to solar values for 27 chemical elements as a function of their condensation temperature. The existing dependence can be traced even by eye. The abundances of elements whose condensation temperature is below 800 K (volatiles) are close to the solar values, and the abundances of elements with a condensation temperature higher than 1000 K (refractory elements) are mainly underabundant. It is interesting to note that the volatile lithophile elements (Na, Zn) show higher abundances compared to other volatile elements (C, N, O, including volatile siderophile S). This is in accordance with the abundances found in chondrites

Table 4. Parameters of the lithium-rich classical Cepheids.

Star	Mode	Period days	$\langle V \rangle$ mag	R_G kpc	d pc	l deg	b deg	Remarks
Galaxy:								
OGLE GD-CEP-0516	P2/P1	0.394959 (P1)	12.666	7.87	2720	285.50	-1.45	Kovtyukh (2023)
ASAS 075842-2536.1	P2/P1	0.41013 (P1)	12.260	9.03	2100	243.55	+2.35	Kovtyukh et al. (2019)
V363 Cas	P2/P1	0.546597 (P1)	10.550	8.76	1155	118.46	-2.22	Catanzaro et al. (2020)
ASAS 131714-6605.0	P2/P1	0.913165 (P1)	11.820	6.85	2200	305.86	-3.64	Kovtyukh et al. (2019)
V371 Per	P1/P0	1.738 (P0)	10.930	10.61	3200	146.02	-14.65	Kovtyukh et al. (2016)
V1033 Cyg	P0	4.9375119	13.027	7.52	3429	69.94	+0.49	Luck & Lambert (2011)
V708 Car	P0	51.403084	12.098	8.24	4378	284.34	-2.43	this paper
LMC:								
HV 5497	P0	99.156076	11.930	-	-	277.24	-36.17	Luck & Lambert (1992)

Remarks: R_G is the galactocentric distance, and d is the heliocentric distance.

Table 5. Parameters of the lithium-rich non-variable supergiants.

HD	Sp	V mag	B-V mag	$v \sin i$ km s ⁻¹	M_V mag	T_{eff} K	$\log g$	V_t km s ⁻¹	[Fe/H] dex	(Li/H)	Remarks
174104	G0Ib	8.37	0.690	50.0	-0.69	5854	2.6	5.0	0.16	3.46	Luck (1982)
172365	F8II	6.36	0.735	67.3	-2.35	5978	1.3	7.5	-0.07	2.90	Luck (1982), Andrievsky et al. (1999)

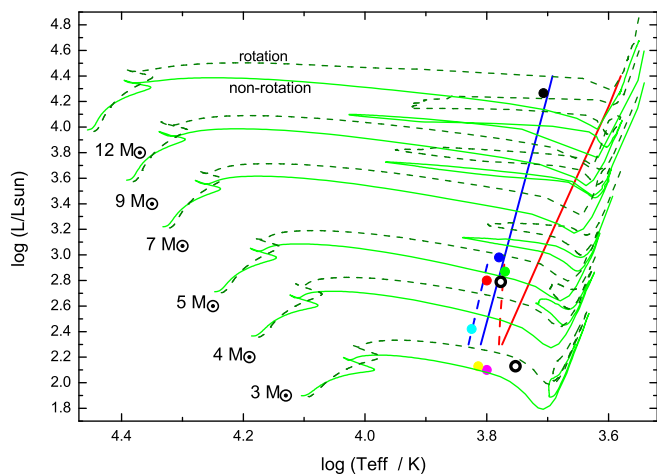


Fig. 3. HR diagram. The positions of our program Cepheid (black circle) and other lithium Cepheids described in the literature are indicated (V371 Per, blue; V1033 Cyg, green; ASAS 131714-6605.0, red; V363 Cas, cyan; ASAS 075842-2536.1, yellow; OGLE GD-CEP-0516, magenta circles; and two nonvariable supergiants, open circles). We plot the evolutionary tracks from Ekström et al. (2012) for 3–12 solar masses with and without rotation. The solid and dashed lines denote the blue and red boundaries of the instability strip for the usual classic Cepheids and so-called s-Cepheids (first-overtone Cepheids have sinusoidal light curves), respectively.

(Wood et al. 2019). According to Wood et al. (2019), lithophile refractory elements (e.g. Mg, Al, Si, Ca, Sc, Ti, Zr, rare-earth elements, and Eu) in chondrites are much more abundant than volatile elements, while refractory siderophile elements (e.g. V, Cr, Mn, Fe, Ni, Co, and Cu) have similar abundances. In the case of our program star, the former and latter groups of elements show much lower abundances than the volatiles. This testifies

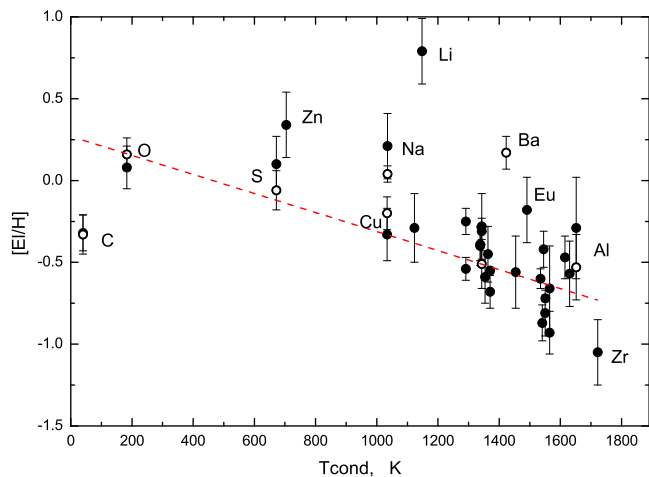


Fig. 4. Element abundances relative to solar in V708 Car as a function of the condensation temperature (LTE is shown as filled circles, and NLTE is shown as open circles). The correlation coefficient is 0.593 (0.669 without Li i).

that some processes occurred in their environment that caused the apparent deficiency of these elements.

According to the definition of Wood et al. (2019), volatility is conventionally defined geochemically in a very broad sense as being related to the temperature at which a specific element would condense from a gas of solar composition. Thus, volatile elements are defined as those that condense at relatively low temperature (e.g., less than 1100 K) from the putative solar gas while refractory, involatile elements condense at higher temperatures.

One of the reasons for the dependence of the abundances of elements on their condensation temperature can be understood considering the chemical anomalies of the λ Boo-type stars, W Vir stars, and post-asymptotic giant branch (post-AGB) stars.

For all these objects, the elemental abundance distribution versus condensation temperature is qualitatively similar and follows the trend described above. The mechanism that explains the chemical peculiarities of these stars has been discussed in several papers. It is based on the assumption that the stellar atmospheres were contaminated by the material of a circumstellar shell. To reach this specific chemical composition, we need to assume that the gas of a circumstellar envelope experienced a separation of dust and gas. Refractory elements can form dust particles at a quite high temperature, and then they can be swept out of the envelope by radiative pressure from the star. The volatile elements stay in the gaseous fraction of the envelope, and the subsequent selective accretion of these elements by the star leads to the specific chemical property of the envelope. The atmosphere of the star becomes deficient in refractory elements and has a normal abundance of volatile elements. In the case of Cepheids, this is true at least for the abundances of elements such as oxygen, sulfur, and zinc because the abundances of carbon and nitrogen can be altered during the first dredge-up episode (carbon is deficient, while nitrogen is overabundant).

For example, the mechanism of the dust–gas separation was applied to explain the chemical peculiarities seen in λ Boo-type stars (see, e.g. Venn & Lambert 1990, Charbonneau 1991, Charbonneau 1993, Sturenborg 1993, Andrievsky 1997, Andrievsky & Paunzen 2000, Andrievsky 2006, Venn & Lambert 2008). Sodium has a rather high condensation temperature, but is often overabundant (like in our program star, as can be seen from Fig. 4). Andrievsky (2006) explained this observed fact in λ Boo-type stars by the specific ionization regime of the sodium atoms that is established in the circumstellar envelope. The same mechanism might be valid for barium, which has a fairly high condensation temperature, but is apparently overabundant. Sodium and barium both have very similar first ionisation potentials of about 5 eV. However, it is unclear why many other chemical elements with a first ionisation potential slightly higher than that of sodium and barium are deficient.

λ Boo-type stars are A–F stars. However, the process of dust–gas separation can be also efficient for G stars. For example, Maas et al. (2007), Kovtyukh et al. (2018) found similar trends for type II Cepheids. A similar depletion pattern was also described by Oomen et al. (2019) for several post-AGB stars. These authors modelled the re-accretion of gas from a dusty circumstellar disc.

As a consequence of the dust–gas separation (Yushchenko et al. 2022), the dust particles that are swept out of the envelope can form coagulated planetesimals. For instance, Meléndez et al. (2009) and Ramírez et al. (2009) showed that our Sun has a small deficiency of refractory elements compared to solar twins, and this may indicate that some fraction of the material containing refractory elements was bound in the planets.

An indirect indication of the presence of a circumstellar envelope (or extended atmosphere) for classical Cepheids exists in the literature. However, the origin of these structures as envelopes or extended atmospheres in these stars is unknown. One solution of the problem could be permanent mass loss either at the stage of a red supergiant or at the later stage of a Cepheid. A similar mechanism was used by van Loon et al. (2005), who showed that the mass-loss rate increases with increasing luminosity of the star (we recall that our program star is very luminous; see the Introduction). It is interesting to note that according to Kervella et al. (2019), the long-period Cepheid RS Pup is embedded in the dusty circumstellar nebula, but its origin is unclear.

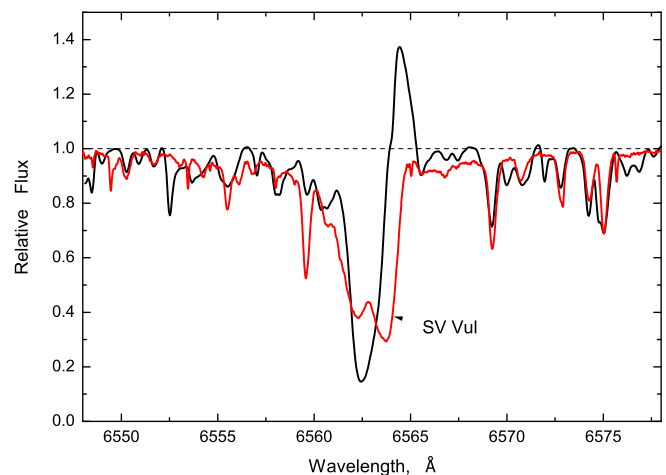


Fig. 5. $H\alpha$ profile in the spectrum of V708 Car (solid black line). For comparison, the spectrum of the Cepheid SV Vul ($P = 44.89$ d, solid red line) is shown, whose parameters are similar to those of V708 Car, and which was observed in the same pulsation phase 0.22.

Our program star has strong $H\alpha$ emission (see Fig. 5). This emission may serve as indirect evidence of the gaseous envelope surrounding V708 Car. The 2MASS all-sky catalogue (Cutri et al. 2003) lists the magnitudes of V708 Car in different bands. The star appears very bright in the H and K bands (about 6 mag), but is quite faint in the V band (about 12 mag).

Since V708 Car is situated at the blue edge of the Cepheid instability strip (Fig. 3), convection probably had no time to erase atmospheric chemical peculiarities. Its pulsation amplitude is small (0.55 mag in V band; Berdnikov 2010), and this could be additional evidence that this star is just at the border of the instability strip. However, we stress again that Berdnikov (2010) considered this star to be at its third crossing of the instability strip.

We lack information about the properties of the present-day envelope of V708 Car, including temperature or the density–pressure distributions. This is probably not very important, however, because the mechanism of the gas–dust separation described above could have occurred earlier, at the MS stage, or immediately after it. The position of V708 Car in the HR diagram (Fig. 3) indicates that its mass is rather high, so that it could be formed as a result of the evolution of two stars. For example, if two MS intermediate-mass B stars (with masses of about 7 and 5 solar masses, e.g.) were to undergo a common evolution in a binary system with mass transfer, the result of this process would be a B (super)giant star with a mass of about 12 solar masses (and with a merged or unmerged white dwarf that previously was the primary component). It is possible that during this evolution, a common envelope forms. Since B stars do not have convective zones in their outer atmosphere, their atmospheres are affected by the gas–dust separation in the envelope and will retain a chemical anomaly for a long time. This situation will not change after the further excursion of the star that formed in this way to the instability strip. We probably observe V708 Car in this stage.

We cannot reproduce the physical conditions in the relic envelope of V708 Car. We therefore applied the widely used condensation temperatures provided by Lodders (2003). They are given for a pressure of 10^{-4} bar. According to the Gay-Lussac law, pressure is linearly proportional to temperature. For any local value of pressure in the envelope, the overall picture of the

condensation temperatures for different species therefore scales proportionally.

5. Conclusion

We discovered and described the lithium-rich Cepheid V708 Car ($\log A(\text{Li}) = 1.95$), which together with six already known lithium Cepheids and two lithium-rich non-variable supergiants forms a small group of lithium-rich yellow supergiants. Our program star also exhibits an anomalous chemical composition. The measured abundances of the chemical elements show a clear correlation with their condensation temperature. We explained this phenomenon as the result of dust–gas separation in the envelope (or extended atmosphere) of V708 Car. Through this mechanism, refractory elements form dust grains in the envelope that are swept out of the envelope by the radiative pressure of the star. The gaseous fraction, enriched in volatile elements, is accreted by the star, and eventually, its atmosphere acquires the observed peculiarity.

We probably caught the star at a very short-term evolutionary stage of interaction with the shell.

Acknowledgements. SMA would like to acknowledge the support from the ESO Scientific Visitor Programme. The authors thank the anonymous referee for their careful reading of the paper and for their comments, which improved the clarity of our manuscript. All observations reported in this paper were obtained within observational program 2016-1-MLT-002 at the Southern African Large Telescope (SALT). AK acknowledges the National Research Foundation (NRF) of South Africa. This research has made use of the SIMBAD database, operated at CDS, Strasbourg, France.

References

- Andrievsky, S. M. 1997, *A&A*, 321, 838
 Andrievsky, S. M. 2006, *A&A*, 449, 345
 Andrievsky, S. M., Gorlova, N. I., Klochkova, V. G., Kovtyukh, V. V., & Panchuk, V. E. 1999, *Astronomische Nachrichten*, 320, 35
 Andrievsky, S. M., Kovtyukh, V. V., Korotin, S. A., Spite, M., & Spite, F. 2001, *A&A*, 367, 605
 Andrievsky, S. M., Martin, R. P., Kovtyukh, V. V., Korotin, S. A., & Lépine, J. R. D. 2016, *MNRAS*, 461, 4256
 Andrievsky, S. M. & Paunzen, E. 2000, *MNRAS*, 313, 547
 Andrievsky, S. M., Spite, M., Korotin, S. A., et al. 2008, *A&A*, 481, 481
 Andrievsky, S. M., Spite, M., Korotin, S. A., et al. 2009, *A&A*, 494, 1083
 Asplund, M., Grevesse, N., Sauval, A. J., & Scott, P. 2009, *ARA&A*, 47, 481
 Barnes, S. I., Cottrell, P. L., Albrow, M. D., et al. 2008, in *Society of Photo-Optical Instrumentation Engineers (SPIE) Conference Series*, Vol. 7014, *Ground-based and Airborne Instrumentation for Astronomy II*, ed. I. S. McLean & M. M. Casali, 70140K
 Berdnikov, L. N. 2010, *Astronomy Letters*, 36, 569
 Bramall, D. G., Schmoll, J., Tyas, L. M. G., et al. 2012, in *Society of Photo-Optical Instrumentation Engineers (SPIE) Conference Series*, Vol. 8446, *Ground-based and Airborne Instrumentation for Astronomy IV*, ed. I. S. McLean, S. K. Ramsay, & H. Takami, 84460A
 Bramall, D. G., Sharples, R., Tyas, L., et al. 2010, in *Society of Photo-Optical Instrumentation Engineers (SPIE) Conference Series*, Vol. 7735, *Ground-based and Airborne Instrumentation for Astronomy III*, ed. I. S. McLean, S. K. Ramsay, & H. Takami, 77354F
 Breuval, L., Riess, A. G., Kervella, P., Anderson, R. I., & Romaniello, M. 2022, *ApJ*, 939, 89
 Buckley, D. A. H., Swart, G. P., & Meiring, J. G. 2006, in *Society of Photo-Optical Instrumentation Engineers (SPIE) Conference Series*, Vol. 6267, *Ground-based and Airborne Telescopes*, ed. L. M. Stepp, 62670Z
 Caffau, E., Monaco, L., Bonifacio, P., et al. 2019, *A&A*, 628, A46
 Carlsson, M. 1986, *Uppsala Astronomical Observatory Reports*, 33
 Castellì, F. & Kurucz, R. L. 2003, in *Modelling of Stellar Atmospheres*, ed. N. Piskunov, W. W. Weiss, & D. F. Gray, Vol. 210, A20
 Catanzaro, G., Ripepi, V., Clementini, G., et al. 2020, *A&A*, 639, L4
 Charbonneau, P. 1991, *ApJ*, 372, L33
 Charbonneau, P. 1993, *ApJ*, 405, 720
 Crause, L. A., Sharples, R. M., Bramall, D. G., et al. 2014, in *Society of Photo-Optical Instrumentation Engineers (SPIE) Conference Series*, Vol. 9147, *Ground-based and Airborne Instrumentation for Astronomy V*, ed. S. K. Ramsay, I. S. McLean, & H. Takami, 91476T
 Crawford, S. M., Still, M., Schellart, P., et al. 2010, in *Society of Photo-Optical Instrumentation Engineers (SPIE) Conference Series*, Vol. 7737, *Observatory Operations: Strategies, Processes, and Systems III*, ed. D. R. Silva, A. B. Peck, & B. T. Soifer, 773725
 Cutri, R. M., Skrutskie, M. F., van Dyk, S., et al. 2003, *VizieR Online Data Catalog*, II/246
 da Silva, R., Crestani, J., Bono, G., et al. 2022, *A&A*, 661, A104
 Dobrovolskas, V., Kučinskas, A., Bonifacio, P., et al. 2014, *A&A*, 565, A121
 Ekström, S., Georgy, C., Eggenberger, P., et al. 2012, *A&A*, 537, A146
 Gaia Collaboration, Brown, A. G. A., Vallenari, A., et al. 2021, *A&A*, 649, A1
 Kervella, P., Gallenne, A., Evans, N. R., et al. 2019, *A&A*, 623, A117
 Kniazev, A. Y., Usenko, I. A., Kovtyukh, V. V., & Berdnikov, L. N. 2019, *Astrophysical Bulletin*, 74, 208
 Korotin, S. A. 2009, *Astronomy Reports*, 53, 651
 Korotin, S. A., Andrievsky, S. M., & Luck, R. E. 1999, *A&A*, 351, 168
 Korotin, S. A. & Mishenina, T. V. 1999, *Astronomy Reports*, 43, 533
 Kovtyukh, V., Lemasle, B., Bono, G., et al. 2022, *MNRAS*, 510, 1894
 Kovtyukh, V., Lemasle, B., Chekhonadskikh, F., et al. 2016, *MNRAS*, 460, 2077
 Kovtyukh, V., Lemasle, B., Kniazev, A., et al. 2019, *MNRAS*, 488, 3211
 Kovtyukh, V., Yegorova, I., Andrievsky, S., et al. 2018, *MNRAS*, 477, 2276
 Kovtyukh, V. V. 2007, *MNRAS*, 378, 617
 Kovtyukh, V. V. 2023, *Odessa Astronomical Publications*, 36, 64
 Lemasle, B., Hajdu, G., Kovtyukh, V., et al. 2018, *A&A*, 618, A160
 Lodders, K. 2003, *ApJ*, 591, 1220
 Luck, R. E. 1982, *PASP*, 94, 811
 Luck, R. E. 2018, *AJ*, 156, 171
 Luck, R. E. & Lambert, D. L. 1992, *ApJS*, 79, 303
 Luck, R. E. & Lambert, D. L. 2011, *AJ*, 142, 136
 Lyubimkov, L. S., Lambert, D. L., Korotin, S. A., Rachkovskaya, T. M., & Poklad, D. B. 2015, *MNRAS*, 446, 3447
 Maas, T., Giridhar, S., & Lambert, D. L. 2007, *ApJ*, 666, 378
 Meléndez, J., Asplund, M., Gustafsson, B., & Yong, D. 2009, *ApJ*, 704, L66
 Mishenina, T. V., Soubiran, C., Kovtyukh, V. V., & Korotin, S. A. 2004, *A&A*, 418, 551
 O’Donoghue, D., Buckley, D. A. H., Balona, L. A., et al. 2006, *MNRAS*, 372, 151
 Oomen, G.-M., Van Winckel, H., Pols, O., & Nelemans, G. 2019, *A&A*, 629, A49
 Pojmanski, G. 2002, *Acta Astron.*, 52, 397
 Ramírez, I., Meléndez, J., & Asplund, M. 2009, *A&A*, 508, L17
 Ryabchikova, T., Piskunov, N., Kurucz, R. L., et al. 2015, *Phys. Scr*, 90, 054005
 Skowron, D. M., Skowron, J., Mróz, P., et al. 2019, *Acta Astron.*, 69, 305
 Sturenburg, S. 1993, *A&A*, 277, 139
 Tsybal, V., Ryabchikova, T., & Sitnova, T. 2019, in *Astronomical Society of the Pacific Conference Series*, Vol. 518, *Physics of Magnetic Stars*, ed. D. O. Kudryavtsev, I. I. Romanyuk, & I. A. Yakunin, 247–252
 van Loon, J. T., Marshall, J. R., & Zijlstra, A. A. 2005, *A&A*, 442, 597
 Černiauskas, A., Kučinskas, A., Klevas, J., et al. 2017, *A&A*, 604, A35
 Venn, K. A. & Lambert, D. L. 1990, *ApJ*, 363, 234
 Venn, K. A. & Lambert, D. L. 2008, *ApJ*, 677, 572
 Wang, S., Chen, X., de Grijs, R., & Deng, L. 2018, *ApJ*, 852, 78
 Wood, B. J., Smythe, D. J., & Harrison, T. 2019, *American Mineralogist*, 104, 844
 Yushchenko, A., Doikov, D., Andrievsky, S., et al. 2022, *Journal of Astronomy and Space Sciences*, 39, 169